Article

Not peer-reviewed version

A Two-Stage Twisted Blade μ-Vertical Axis Wind Turbine – An Enhanced Savonius Rotor Design

Andrés Pérez-Terrazo , Martin Moreno * , Iván Trejo-Zúñiga * , J. Alberto López

Posted Date: 2 March 2024

doi: 10.20944/preprints202402.1655.v1

Keywords: VAWT; Energy Harvesting; Two-Stage Design; Renewable Energy; Wind Technology

 doi:10.20944/preprints202402.1655.v1

Article

A Two-Stage Twisted Blade μ-Vertical Axis Wind Turbine – An Enhanced Savonius Rotor Design

Andrés Pérez-Terrazo [1,2], Martin Moreno [1,2,*], Iván Trejo-Zúñiga [1,2,*] and J. Alberto López [1]

[1] Universidad Tecnológica de San Juan del Río, San Juan del Río, 76800 Querétaro, México
[2] Laboratory of Energy Innovation and Intelligent and Sustainable Agriculture (LEIISA)
* Correspondence: mmorenog@utsjr.edu.mx (M.M.); itrejoz@utsjr.edu.mx (I.T.-Z.)

Abstract: Wind turbines are a solution for sustainable energy, significantly reducing carbon emissions and fostering a circular economy for more cost-effective and cleaner power generation, in line with worldwide environmental aspirations. In this context, this research aims to explore a novel Two-Stage Twisted Blade micro-Vertical Axis Wind Turbine (μ-VAWT) alternative inspired by the Savonius Rotor (SR). This investigation utilizes the $\kappa - \omega$ SST turbulence model to explore the power coefficient (C_P) and torque coefficient (C_T), finding C_P values ranging from 0.02 to 0.04 across the turbine by altering the free stream velocity (V). C_T analysis further delves into four specific sections, highlighting areas of particular interest. These results are validated by examining velocity contours, pressure contours, and streamlines in four horizontal sections, demonstrating that the proposed turbine model exhibits minimal torque fluctuation. Moreover, the analysis of vertical wind streamlines illustrates very low interference with various wind turbine proposals, underscoring the turbine's efficiency and potential for integration into diverse wind energy projects.

Keywords: VAWT; energy harvesting; two-stage design; renewable energy; wind technology

1. Introduction

Integrating vertical axis wind turbines (VAWT) into our energy systems as a harvesting technology is a forward-thinking approach to sustainability. Unlike their horizontal counterparts, VAWT capture wind from any direction, making them suitable for urban and spatially restricted environments. Using these harvesting technologies to harness wind power diversifies our renewable energy sources, marking an essential step in the fight against climate change. Deploying VAWT indicates a strategic shift towards low-carbon solutions, demonstrating their ability to reduce reliance on fossil fuels, cut greenhouse gas emissions, and promote environmental responsibility [1–3]. Harvesting energy on a small scale is a viable and energy-efficient approach that can enhance the energy utilization of silicon-based electronics, particularly in systems that consume low power [4]. Currently, batteries are the primary power source for these devices. Implementing energy harvesting techniques presents an opportunity to prolong the operational life of these devices and diminish the need for maintenance by eliminating the need to replace batteries. The emergence of small-scale wind energy harvesting (SSWEH) is proving to be a promising and adaptable alternative that can be customized to various environmental conditions [5]. The efficiency of these SSWEH systems is directly proportional to their electrical power generation capacity, which can be sustained over time. This sustainable method introduces diverse energy sources for low-power electronics, making it an attractive option for modern technology. A principal benefit of SSWEH is its decentralized nature as an energy source. This decentralization facilitates local power generation, which reduces dependence on centralized power grids and improves the power supply, especially in remote or underserved areas [6,7]. It also helps reduce transmission losses and the overall environmental impact of large-scale power distribution systems. In small-scale wind energy, the focus often shifts towards the VAWT, with the SR being a prevalent choice [8].

The SR, conceptualized by Sigurd Savonius, represents a distinctive VAWT form. Characterized by its two or more curved blades, colloquially known as "scoops," the turbine operates around a

 doi:10.20944/preprints202402.1655.v1

vertical axis. This design allows the wind to exert more force on the concave side of each blade while encountering less resistance on the convex side, facilitating rotational motion. One of the key advantages of the SR is its proficiency in capturing wind from various directions, obviating the need for reorientation [9]. These advantages are particularly suitable for areas with inconsistent and changeable wind patterns. However, this design has challenges, notably in power and torque (T). A significant limitation is its lower C_P, which hampers energy conversion. Some studies [10] describe the SR disadvantages in its C_T, particularly negative values at certain rotational angles. These fluctuations contribute to increased mechanical vibrations and impact the self-starting capabilities of the rotor.

Additionally, other studies have focused on various rotor modifications and the implementation of multistage rotors. These alterations enhance the rotor performance by reducing negative T. Researchers have conducted various studies comparing the performance of different SR designs, including Bach, Benesh, twisted blades, sine, and conical profiles [11,12]. For example, the research findings in [11] indicate that the sine profile design results in a marginal reduction of the maximum C_P by approximately 1.25% compared to the standard design. Whereas the conical rotor design significantly improves this coefficient by 8.6%. These results suggest that the conical design substantially improves performance compared to traditional SR, highlighting its potential for more effective energy generation. It is worth noting that different shapes impact factors such as T and C_P. Reference [12] provides a comprehensive view of these factors.

In environments with non-constant and low wind conditions, multistage SR has been established as a suitable solution, as demonstrated in [13]. In addition, optimization of variables such as blade pitch angle, twist angle (φ), and overlap ratio has significantly increased T and C_Ps, a finding supported by [13,14]. The results presented in [15,16] indicate that the number of blades in a multistage configuration is a factor that improves the T and C_P. In particular, models with two blades have been found to outperform those with three or four blades in T and power. Simulations highlight the impact of the number of blades on performance, with optimal power conversion occurring at specific tip-speed ratios (TSRs). However, these studies also highlight a trade-off, suggesting that increasing the number of stages can reduce the C_P, underscoring the need for a trade-off between consistent T and energy generation. Integrating intermediate plates in rotor designs adds further complexity to the analysis, as explored in [17]. Additionally, [18] has identified that the phase shift angle (PSA) between stages of multi-rotor is another variable impacting the C_P, demonstrating its beneficial effects.

Likewise, this study provides an aerodynamic evaluation of a uniquely designed microturbine, as illustrated in Figure 1. The turbine is distinguished by its innovative design, featuring two twisted blades with φ set at an angle of 24° each, adhering to the principles of SR design. Furthermore, it boasts a two-stage configuration with a PSA of 65°. The PSA has an essential role in improving the turbine's performance. It does so by facilitating improved wind capture and mitigating the adverse effects of interference between the blades across different stages. This setup aims to optimize the turbines by leveraging the synergistic effects of its design features through the evaluation of the geometric design and its impact on the C_P and C_T. It is done by the development of a comprehensive three-dimensional, incompressible unsteady Reynolds-averaged Navier-Stokes model integrated with the $\kappa - \omega$ shear-stress transport turbulence model, aimed at predicting the effects of variables such as PSA and V on its performance. In this sense, the flow field characteristics are analyzed for assessing the aerodynamic performance impacts due to geometric alterations on the proposal, marking a significant contribution to the understanding of its aerodynamics by employing assessment methods based on flow field characteristics, such as streamlines and pressure fields around the SR, are conducted. The manuscript is organized into five detailed sections, ensuring a logical flow and comprehensive coverage of the research findings. In Section 2, the paper explains the proposed wind turbine's innovative features, specifically focusing on its mechanical configuration. Following this, Section 3 rigorously validates the functionality of the wind turbine by utilizing computational fluid dynamics alongside simulation methodologies. Section 4 examines the achieved aerodynamic performance metrics, highlighting significant findings. The study culminates in Section 5, which summarizes

 doi:10.20944/preprints202402.1655.v1

insights and conclusions drawn from the research. This structured approach facilitates a clear and thorough understanding of the study's contributions.

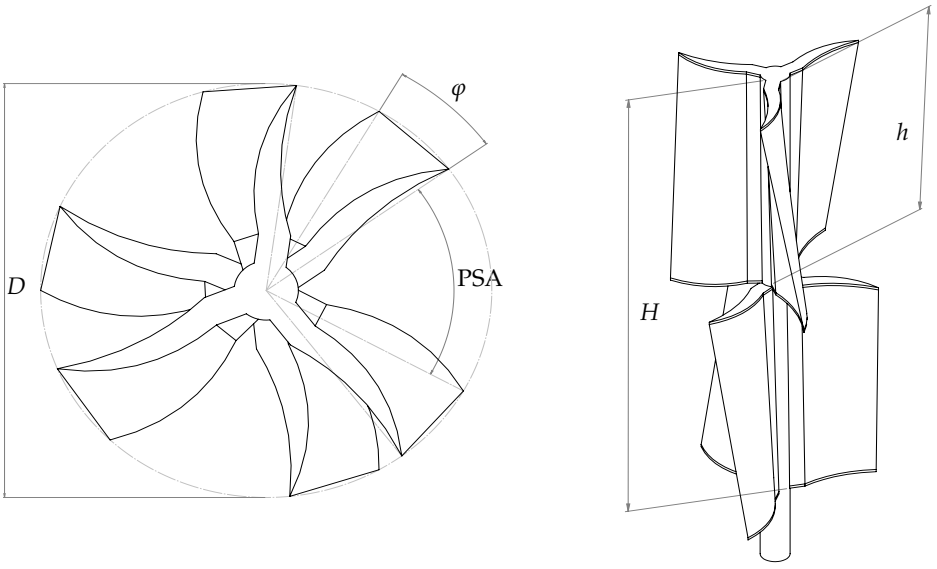

Figure 1. Dimension of a Two-Stage Twisted Blade μ-VAWT. a) View from the Top Plane. b) View from the Vertical Plane.

2. Features and Design for Two-Stage Twisted Blade Wind Turbine

Several geometric factors, including the number of blades, twist angles, and the position of the PSA, influence the performance of multi-stage SRs. In this context, in [15] investigated the mechanical design aspects of two-, three-, and four-bladed systems within two-stage SRs without considering twisted blades. The study identified that a three-bladed configuration with a PSA of 90° and an optimal tip speed ratio λ value of 0.8 was the most efficient. Meanwhile, the work [16] examined multi-stage SRs but did not consider SR plates or twisted blades. The study introduced unconventional PSA values and documented thrust coefficients C_T and C_P across various stages, highlighting turbulent flow patterns around the SR with notable vorticity. Contrarily, the authors in [13] use a two-bladed system with blades twisted at a $\varphi = 45°$ angle and a PSA of 90°. Researchers have found that a two-stage SR with twisted blades consistently maintains a positive static coefficient torque C_{TS} throughout its revolution, which improves the rotor's self-starting capabilities and identifies an optimal λ of 0.8. Based on these insights, this study introduces a design with a three-bladed configuration tested at a $\varphi = 25°$ with a PSA of 65°, intentionally omitting plates from its design. This approach suggests a new direction in SR design by incorporating specific geometric modifications to upgrade the performance, as Figure 1.a shows. The design defines each stage with a height of 90 mm, leading to a total height of 180 mm for the two-stage turbine, and it features a specific size ratio as depicted in Figure 1.b. The rotor diameter remains a standard 70 mm across both models, serving low-power load applications as detailed in the Table 1.

 doi:10.20944/preprints202402.1655.v1

Table 1. Dimension parameters of two-stage twisted blade μ-VAWT

Parameter	Magnitud [mm]
h	90
D	70
H	180
Section I	0
Section II	45
Section III	135
Section IV	180

We comprehensively analyzed the C_T values ranging from 15° to 90°. Based on the findings, we concluded that the optimal setting for the PSA is 65°. Figure 2 displays that the C_T reaches an equilibrium state at this angle, significantly improving the system's performance. The symmetrical design of the mechanical structure minimizes unwanted forces, making the 65° PSA the most suitable choice for generating optimal T. We referred to the findings presented in [13] to keep λ at 0.8 during the analysis. This research explores the impact of altering several geometrical parameters, including the φ, the PSA between the stages, and free stream wind speed (V), on the performance of the proposed twisted ST. The rotor diameter is maintained at a constant 70 mm, featuring a 3 to 1 mm thickness and an aspect ratio ($AR = H/D$) set at "2.5". The twist angles under examination include 0^o, 45^o, 90^o and 180^o. Figure 3 illustrates the definition of the PSA. The last scrutinized geometric parameter pertains to the AR of the blades in each stage. With twists, the two-stage SR experiences a V ranging from 2 to 15 m/s.

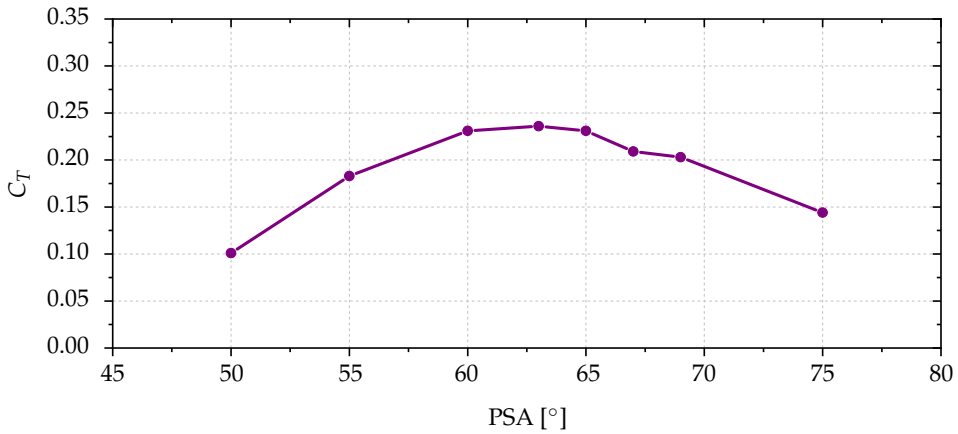

Figure 2. Optimization of PSA for two-stage twisted blade μ-VAWT at $V = 7\,m/s$

 doi:10.20944/preprints202402.1655.v1

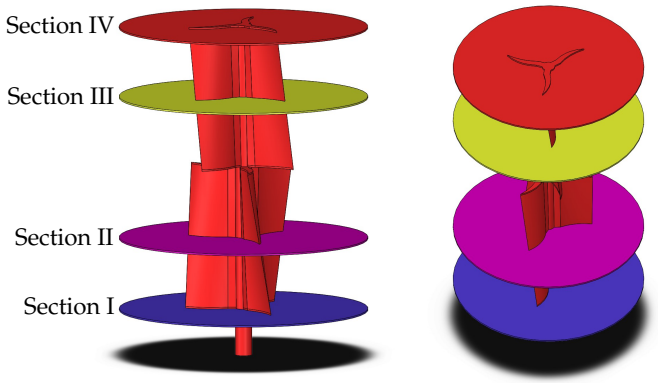

(a) (b)

Figure 3. Mechanical Design of a Two-Stage Twisted Blade μ-VAWT. a) View from the Vertical Plane. b) View from the Top Plane.

3. Validation of the Two-Stage Twisted Blade Wind Turbine Model

In SRs, the C_p as the quotient of the actual power output the rotor (P_{rotor}) produces over the available wind power (P_{wind}), formulated as follows:

$$C_p = \frac{P_{rotor}}{P_{wind}} = \frac{T \times w_r}{0.5\rho A V^3} = \frac{2\pi N T}{60 \times 0.5\rho A V^3} \tag{1}$$

Static torque (T_s) is called the net T of the rotor under static conditions and is mainly responsible for the starting capacity of the rotor. Dynamic T denotes the operating load of the rotor while in motion, which significantly influences its power conversion capability. The C_{TS} and dynamic C_T coefficients are defined as:

$$C_{TS} = \frac{4T_S}{\rho V^2 D^2 H} \tag{2}$$

$$C_T = \frac{4T}{\rho V^2 D^2 H} \tag{3}$$

The λ is defined as the ratio between rotor tip speed (u_t) and V and is given by:

$$\lambda = \frac{u_t}{V} \tag{4}$$

3.1. Computational Fluid Dynamic

Numerical simulations of the two-stage twisted-blade SR were formed with ANSYS CFD using the Finite Volumes Method, which uses the conservation equations of mass and momentum Reynolds Average Navier-Stokes Equations (RANS). It is possible to make a substitution in the principle of conservation of mass through the Reynolds decomposition, which consists of decomposing a scalar or vector variable into an average temporal part and another as a fluctuating part,

$$u(t) = \bar{u} + u'(t) \tag{5}$$

$$\frac{\partial \bar{u}_i}{\partial x_i} = 0 \tag{6}$$

 doi:10.20944/preprints202402.1655.v1

The momentum equilibrium equation can be obtained by the Reynolds decomposition for velocity and pressure using the momentum principle, which is obtained as:

$$\frac{\partial \bar{u_i}}{\partial t} + \bar{u_j}\frac{\partial \bar{u_i}}{\partial x_j} = -\frac{1}{\rho}\frac{\partial \bar{p}}{\partial x_i} + \nu\frac{\partial^2 \bar{u_i}}{\partial x_i \partial x_j} - \frac{\partial}{\partial x_j}\overline{u_i' u_j'} \tag{7}$$

The Reynolds stress tensor, which is a symmetric tensor is composed of correlations described by $\overline{u_i' u_j'}$, can be expressed;

$$-\rho\overline{u_i' u_j'} = \tau \tag{8}$$

To solve the closure problem, the $\kappa - \omega$ SST turbulence model is used. The $\kappa - \omega$ SST model combines the $\kappa - \epsilon$ and $\kappa - \omega$ models. Other authors [19] have demonstrated the formulation based on mixing functions, which ensures an adequate selection of the $\kappa - \omega$ and $\kappa - \epsilon$ zones without user interaction. In each case, a time step value is used according to;

$$\Delta t = \frac{\Delta\theta\pi}{180^\circ w_0} \tag{9}$$

Where $\Delta\theta$ is the angular step and w_0 is the angular velocity.

3.2. Number of cells and domain

Determining the optimal size of the computational is crucial to ensure accurate numerical results while minimizing computational time. The computational domain size is typically described using four parameters: 1) Upstream domain length (X_{up}), which is measured from the inlet faces to the center of the rotor; 2) Downstream domain length (X_{down}), this parameter is measured from the center of the outlet surfaces; 3) Width of the computational domain (Y), it is measured along the Y-axis and 4) Height of the computational domain (Z), this parameter is measured along the Z-axis. The optimal domain size is determined by examining the effects of downstream domain length (Z_{down}), width of the computational domain (Y), and height of the computational domain(Z) on the C_T [20,21].

To minimize the time computing, it is necessary to optimize the number of cells. Therefore, the conditions for varying the number of cells involve defining the cell size of the rotor while maintaining a fixed growth rate of 1.2 for the cell size throughout the computational domain. The accuracy of each model is assessed by measuring the relative error between the current numerical C_P and the experimental results provided by other works [19,22].

In the computational analysis of the two-stage twisted-blade wind turbine, the mesh propagation through the computational domain encompasses 2,474,307 cells, as Figure 4.a demonstrates. This mesh structure is vital in accurately simulating and analyzing the wind turbine's aerodynamic properties. Experts meticulously examine the mesh distribution surrounding the rotor using section planes to gain a deeper understanding of the flow dynamics and turbine performance under various conditions. The current mesh model achieves a relative error of 1.7%. The first sectional analysis in the X-Y plane offers a horizontal cross-sectional view of the mesh distribution around the rotor. This view sheds light on the interaction between the rotor blades and the wind flow in the horizontal plane, leading to the acquisition of a surface rotor of 1 mm, as depicted in Figure 4.b. This analysis aids in evaluating factors like blade tip vortices and horizontal wind shear effects, which are crucial for optimizing the turbine's structural integrity. Similarly, the second sectional analysis, employing the X-Z plane, reveals a vertical cross-sectional view of the mesh distribution, as shown in Figure 4.c.

 doi:10.20944/preprints202402.1655.v1

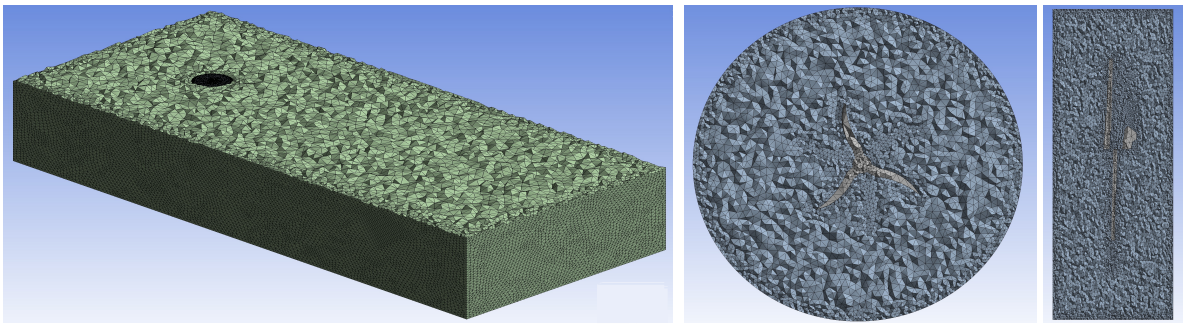

(a) (b) (c)

Figure 4. Mesh Propagation Analysis. a) In the Computational Domain, b) On the X–Y Plane, c) Through the X–Z Plane.

The validation process aims to match the performance of other studies [23], thereby maintaining the operational range Reynolds number (Re). It is critical that the distributions of C_p and C_T with λ at a specific range Re stay independent of the geometry properties [19,21]. Evaluating convergence in the numerical simulations depends on two criteria: i) Minimal variation in the average results of Cp and T, and ii) Consistency in the instantaneous distribution of T over a certain number of cycles. Meeting these criteria ensures that the validation process confirms that the numerical model accurately reflects the performance characteristics of the SR across a wide range of operating conditions.

4. Results

This section investigates how steady wind scenarios affect the performance of a novel wind turbine featuring a twisted blade design and SPA. We examine the rotor performance of this turbine using the methodologies described in [24]. In this context, we present a comprehensive description of velocity contours across horizontal sections at azimuthal angles of $\theta = 0°$, $\theta = 90°$, $\theta = 180°$, and $\theta = 270°$ in the proposed wind turbine (Figure 5). These sections, labeled I, II, III, and IV, act as radial slices at different heights along the turbine's vertical axis (Figure 3). At $\theta = 0°$, Figure 5.a shows the initial interaction between the wind and the blade without rotational effects. Progressing to $\theta = 90°$, Figure 5.b displays an increase in wind velocities at certain sections due to the blade's motion. The velocity distribution at $\theta = 180°$, as shown in Figure 5.c, examines the varied aerodynamic forces on the blade's opposite side after half a rotation, highlighting the effects of recovery and wake. Finally, Figure 5.d at $\theta = 270°$ completes the cycle by showing how the wind interacts with the blade's trailing edges. We understand these variations, caused by the blades' sectional twisting of φ and the PSA employed between stages, as the aerodynamic interactions that dictate turbine operation.

 doi:10.20944/preprints202402.1655.v1

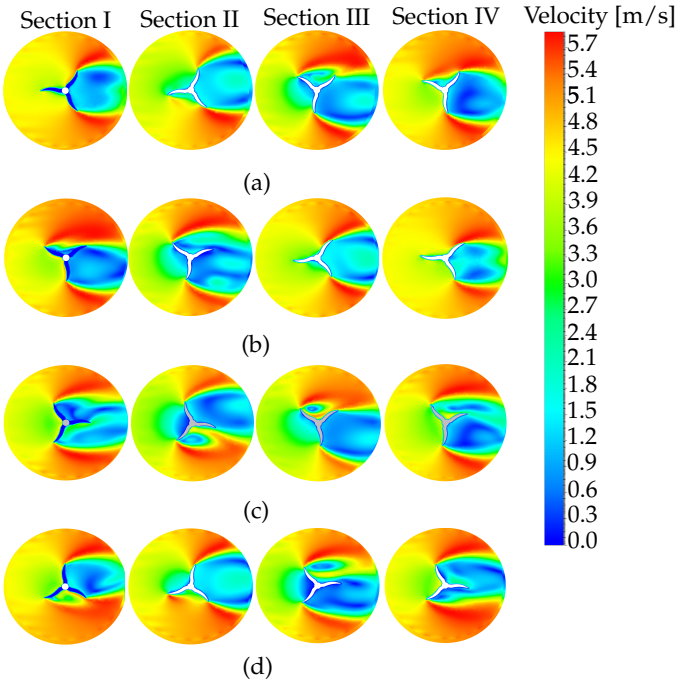

Figure 5. Distribution of Velocity Contours Over Horizontal Sections in a Two-Stage at Four Angles with $V = 5\,m/s$: a) $\theta = 0°$, b) $\theta = 90°$, c) $\theta = 180°$, d) $\theta = 270°$

Figure 6 showcases pressure contour plots for a proposed configuration, illustrating the comprehensive integration of φ and PSA across azimuthal angles $\theta = 0°$, $\theta = 90°$, $\theta = 180°$, and $\theta = 270°$. These plots reveal how the configuration affects pressure distribution across horizontal sections labeled I, II, III, and IV, which correspond to radial slices at varying heights along the turbine's vertical axis (Figure 3). The integration significantly reduces impact pressure in the forward contact area where the wind first encounters the blades. This design feature results in a favorable pressure distribution within the φ, enhancing aerodynamics and reducing the adverse effects of high dynamic pressures. Such strategic force distribution along the blade suggests improved operational stability and decreased structural stress.

Preprints.org (www.preprints.org) | NOT PEER-REVIEWED | Posted: 2 March 2024 doi:10.20944/preprints202402.1655.v1

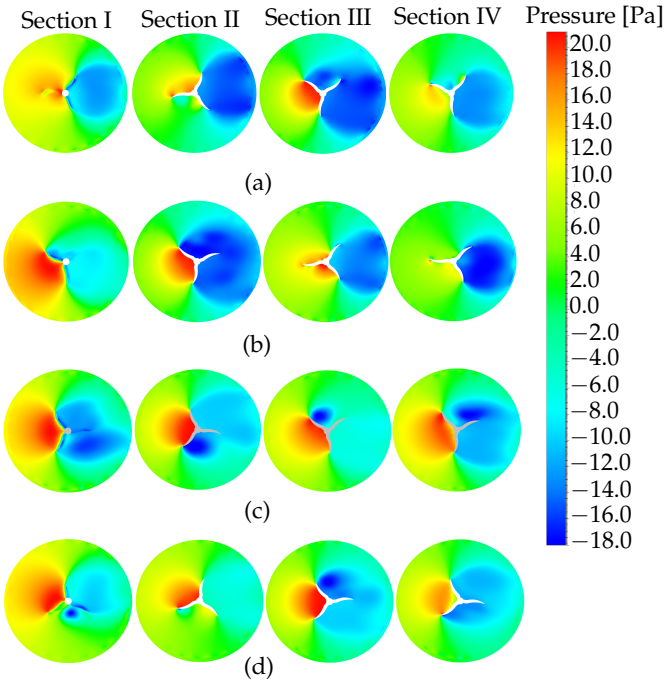

Figure 6. Distribution of Pressure Contours Over Horizontal Sections in a Two-Stage at Four Angles with $V = 5\,m/s$: a) $\theta = 0°$, b) $\theta = 90°$, c) $\theta = 180°$, d) $\theta = 270°$

Figure 7 depicts the distribution of streamlines across four distinct sections. This illustration shows the integration of φ and PSA with the azimuthal angles $\theta = 0°$, $\theta = 90°$, $\theta = 180°$, and $\theta = 270°$. In the vortices, the velocity magnitudes progressively approach values nearing zero in sections advancing towards section IV, which exhibits a simplified flow pattern. The primary reason for this observation is attributed to the symmetry of the PSA about the φ of the blades, suggesting a strong interdependence between the geometric configuration of the blades and the dynamics within the turbine.

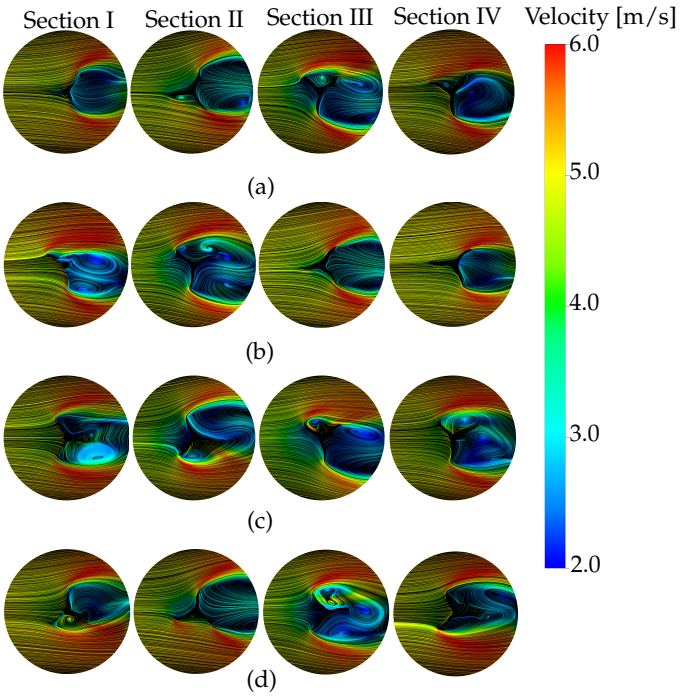

Figure 7. Distribution of Streamlines Over Horizontal Sections in a Two-Stage at Four Angles with $V = 5\,m/s$: a) $\theta = 0°$, b) $\theta = 90°$, c) $\theta = 180°$, d) $\theta = 270°$

 doi:10.20944/preprints202402.1655.v1

The analysis involves a performance evaluation of C_T in different sections, as shown in Figure 8. Figure 8.a, evaluated at a speed of 2 m/s, indicates that sections III and IV have higher amplitudes at $\theta = 180^\circ$ due to their more significant vorticity in comparison to sections I and II. On the other hand, Figure 8.b shows that section IV has a higher amplitude, whereas sections I, II, and III have similar values of C_T. At a speed of 8 m/s, all sections show almost identical C_T values, indicating a well-balanced distribution of streamlines and vorticity, as depicted in Figure 8c. The analysis calculates C_P for each scenario, revealing a favorable correlation with λ.

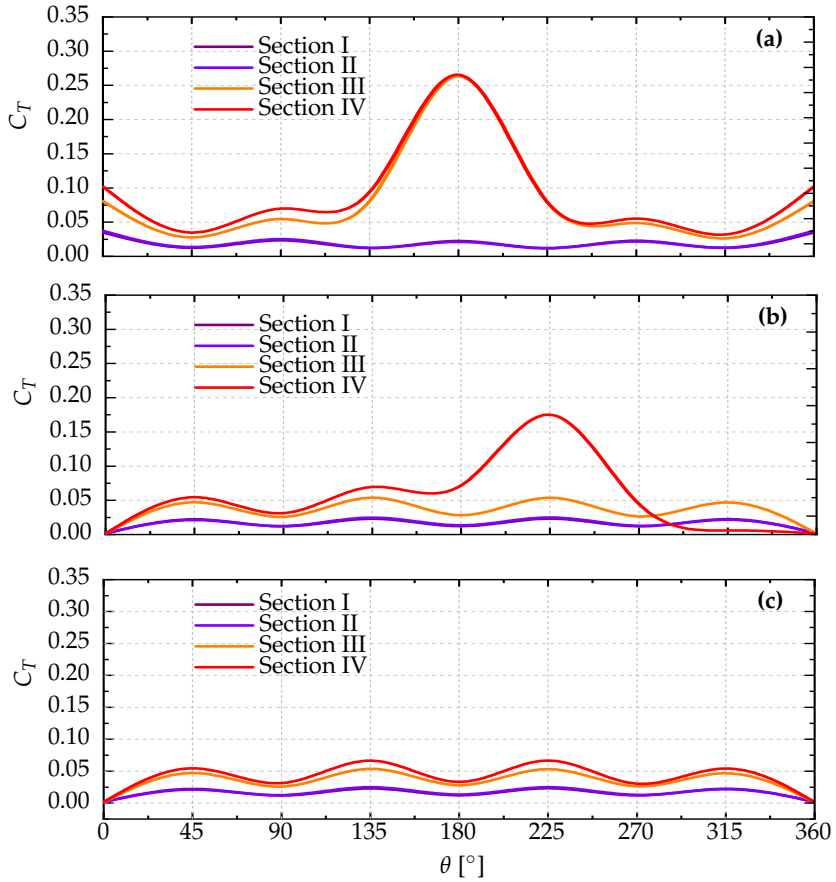

Figure 8. C_T Variation with Rotational-azimuthal angles at λ = 0.8. a) Attaining a C_P value of 0.04 when $V = 2\,m/s$. b) Reaching a C_P value of 0.02 with $V = 5\,m/s$.c) Achieving a C_P value of 0.02 at $V = 8\,m/s$.

5. Conclusions

The study demonstrates the potential of a two-stage turbine with a twisted blade optimized at an aspect ratio of 2.5. Leveraging a three-dimensional model for turbulent flow, grounded in the RANS equations and enhanced by the $\kappa - \omega$ SST turbulence model, the study reveals critical insights. Fine-tuning the PSA between 15° and 70°, the C_T values are between 0.01 and 0.02. They resulted in an ideal PSA of 65° at λ of 0.8. This specific PSA exhibits an oscillatory pattern across positive values and underscores the turbine's inherent self-starting ability, attributed to its strategic design. Confirming the superior C_T at a PSA of 65°, the study dissects the turbine into four horizontal sections, rotating the rotor through 0°, 90°, 180°, and 270° to meticulously observe changes in wind velocity, pressure, and vorticity. The results map out the vorticity's methodical breakdown from Section I through IV. Remarkably, at lower velocities, sections III and IV showcase significantly higher amplitudes at $\theta = 180^\circ$ angle, indicating a pronounced increase in T. At intermediate velocities, the C_T amplitude notably shifts to $\theta = 225^\circ$, harmonizing across all sections at higher speeds.

 doi:10.20944/preprints202402.1655.v1

Additionally, the research explores the potential effects of integrating more turbines for energy harvesting. When viewed from a vertical section, the wind lines quickly come back together, leaving behind a trail with minimal turbulence, as shown in Figure 9. This discovery implies that deploying multiple wind turbines in the suggested configuration could significantly power small loads, such as sensors and low-power instrumentation. This approach is proposed as a viable strategy for the gradual and sustainable decarbonization of the electrical grid by global sustainability and energy efficiency objectives.

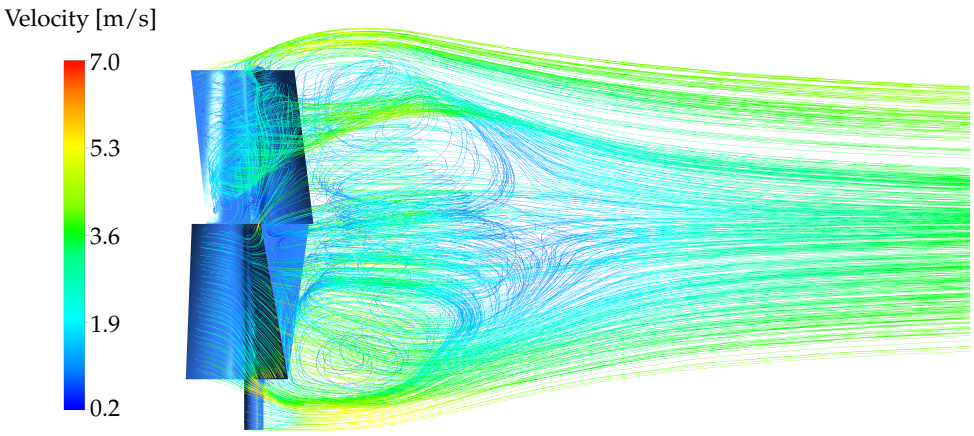

Figure 9. Distribution of Streamlines Over Vertical Section

References

1. Barthelmie, R.J.; Pryor, S.C. Climate Change Mitigation Potential of Wind Energy. *Climate* **2021**, *9*, 136. doi:https://doi.org/10.3390/cli9090136.
2. Sun, C.; Wei, J.; Zhao, X.; Yang, F. Impact of Carbon Tax and Carbon Emission Trading on Wind Power in China: Based on the Evolutionary Game Theory. *Frontiers in Energy Research* **2022**, *9*. doi:10.3389/fenrg.2021.811234.
3. Karnauskas, K.B.; Lundquist, J.K.; Zhang, L. Southward shift of the global wind energy resource under high carbon dioxide emissions. *Nature Geoscience* **2017**, *11*, 38–43. doi:https://doi.org/10.1038/s41561-017-0029-9.
4. Vullers, R.; Schaijk, R.; Visser, H.; Penders, J.; Hoof, C. Energy Harvesting for Autonomous Wireless Sensor Networks. *IEEE Solid-State Circuits Magazine* **2010**, *2*, 29–38. doi:https://doi.org/10.1109/MSSC.2010.936667.
5. Tummala, A.; Velamati, R.K.; Sinha, D.K.; Indraja, V.; Krishna, V.H. A review on small scale wind turbines. *Renewable and Sustainable Energy Reviews* **2016**, *56*, 1351–1371. doi:http://dx.doi.org/10.1016/j.rser.2015.12.027.
6. Notton, G.; Muselli, M.; Poggi, P.; Louche, A. Decentralized wind energy systems providing small electrical loads in remote areas. *International Journal of Energy Research* **2001**, *25*, 141–164. doi:https://doi.org/10.1002/er.670.
7. Calautit, K.; Johnstone, C. State-of-the-art review of micro to small-scale wind energy harvesting technologies for building integration. *Energy Conversion and Management: X* **2023**, *20*, 100457. doi:https://doi.org/10.1016/j.ecmx.2023.100457.
8. Marin, A.; Kishore, R.; Schaab, D.A.; Vuckovic, D.; Priya, S. Micro Wind Turbine for Powering Wireless Sensor Nodes. *Energy Harvesting and Systems* **2015**, *3*, 139–152. doi:http://dx.doi.org/10.1515/ehs-2013-0004.
9. Dewan, A.; Gautam, A.; Goyal, R. Savonius wind turbines: A review of recent advances in design and performance enhancements. *Materials Today: Proceedings* **2021**, *47*, 2976–2983. doi:https://doi.org/10.1016/j.matpr.2021.05.205.
10. Santoso, D.; Riady, M.I.; Yanto, J.; Dwinesa, N.; Fatma, A.N. Performance improvement of savonius wind turbine with geometry modified and blade configuration. AIP Conference Proceedings. AIP Publishing, 2023. doi:https://doi.org/10.1063/5.0114972.

11. Abdelaziz, K.R.; Nawar, M.A.; Ramadan, A.; Attai, Y.A.; Mohamed, M.H. Performance assessment of a modified of Savonius rotor: Impact of sine and conical blade profiles. *Energy* **2023**, *272*, 127172. doi:https://doi.org/10.1016/j.energy.2023.127172.
12. Alom, N.; Saha, U.K. Evolution and Progress in the Development of Savonius Wind Turbine Rotor Blade Profiles and Shapes. *Journal of Solar Energy Engineering* **2018**, *141*. doi:https://doi.org/10.1115/1.4041848.
13. Saad, A.S.; Elwardany, A.; El-Sharkawy, I.I.; Ookawara, S.; Ahmed, M. Performance evaluation of a novel vertical axis wind turbine using twisted blades in multi-stage Savonius rotors. *Energy Conversion and Management* **2021**, *235*, 114013. doi:https://doi.org/10.1016/j.enconman.2021.114013.
14. Patel, U.K.; Alom, N.; Saha, U.K. Aerodynamic analysis of a 2-stage elliptical-bladed Savonius wind rotor: Numerical simulation and experimental validation. *International Journal of Green Energy* **2023**, *21*, 102–115. doi:https://doi.org/10.1080/15435075.2023.2194975.
15. Mohd Halmy, M.S.; Didane, D.H.; Afolabi, L.O.; Al-Alimi, S. Computational Fluid Dynamics (CFD) Study on the Effect of the Number of Blades on the Performance of Double-Stage Savonius Rotor. *CFD Letters* **2021**, *13*, 1–10. doi:https://doi.org/10.37934/cfdl.13.4.110.
16. Frikha, S.; Driss, Z.; Ayadi, E.; Masmoudi, Z.; Abid, M.S. Numerical and experimental characterization of multi-stage Savonius rotors. *Energy* **2016**, *114*, 382–404. doi:https://doi.org/10.1016/j.energy.2016.08.017.
17. Kamoji, M.A. and Kedare, S.B. and Prabhu, S.V.. Experimental Investigations on Two and Three Stage Modified Savonius Rotor. *Wind Engineering* **2011**, *35*, 483–509. doi:https://doi.org/10.1260/0309-524X.35.4.483.
18. Chen, J.; Chen, L.; Nie, L.; Xu, H.; Mo, Y.; Wang, C. Experimental study of two-stage Savonius rotors with different gap ratios and phase shift angles. *Journal of Renewable and Sustainable Energy* **2016**, *8*. doi:http://dx.doi.org/10.1063/1.4966706.
19. Saad, A.S.; El-Sharkawy, I.I.; Ookawara, S.; Ahmed, M. Performance enhancement of twisted-bladed Savonius vertical axis wind turbines. *Energy Conversion and Management* **2020**, *209*, 112673. doi:https://doi.org/10.1016/j.enconman.2020.112673.
20. Abdelaziz, Khaled R. and Nawar, Mohamed A.A. and Ramadan, Ahmed and Attai, Youssef A. and Mohamed, Mohamed H.. Performance improvement of a Savonius turbine by using auxiliary blades. *Energy* **2022**, *244*, 122575. doi:10.1016/j.energy.2021.122575.
21. Ramadan, A. and Yousef, K. and Said, M. and Mohamed, M.H.. Shape optimization and experimental validation of a drag vertical axis wind turbine. *Energy* **2018**, *151*, 839–853. doi:10.1016/j.energy.2018.03.117.
22. Sugiharto, B.; Soeparman, S.; Widhiyanuriyawan, D.; Wahyudi, S. Characteristics of the Savonius Wind Turbine Using Multiple Guide Vanes. *International Journal of Fluid Machinery and Systems* **2020**, *13*, 606–614. doi:10.5293/IJFMS.2020.13.3.606.
23. Song, C.; Wu, G.; Zhu, W.; Zhang, X.; Zhao, J. Numerical Investigation on the Effects of Airfoil Leading Edge Radius on the Aerodynamic Performance of H-Rotor Darrieus Vertical Axis Wind Turbine. *Energies* **2019**, *12*, 3794. doi:https://doi.org/10.3390/en12193794.
24. Scheurich, F.; Fletcher, T.M.; Brown, R.E. Effect of blade geometry on the aerodynamic loads produced by vertical-axis wind turbines. *Proceedings of the Institution of Mechanical Engineers, Part A: Journal of Power and Energy* **2011**, *225*, 327–341. doi:https://doi.org/10.1177/2041296710394248.